Phase Behavior of Styrene−Isoprene Diblock Derivatives with Varying Conformational Asymmetry

Chiajen Lai,† William B. Russel, and Richard A. Register*

Department of Chemical Engineering, Princeton University, Princeton, New Jersey 08544

Gary R. Marchand‡

The Dow Chemical Company, P.O. Box 400, Plaquemine, Louisiana 70765

Douglas H. Adamson

Princeton Materials Institute, Princeton University, Princeton, New Jersey 08540

Received July 16, 1999; Revised Manuscript Received March 2, 2000

ABSTRACT: At present, diblock copolymer phase behavior in the long-chain limit is considered to be governed by three factors: the volume fraction of one block, ϕ; the segregation strength of the diblock, χN; and the conformational asymmetry parameter, ϵ. This implies that the phase diagrams for polymers of different chemistry but similar molecular weight should evolve simply and smoothly as ϵ is varied. We present here partial phase diagrams (covering the cylinder−gyroid−lamella region) for two derivatives of the well-known styrene−isoprene diblocks: styrene−(ethylene-*alt*-propylene) and vinylcyclohexane−(ethylene-*alt*-propylene), all of similar molecular weights. Comparison of the S/I, VCH/EP, and S/EP phase diagrams reveals that the phase behavior does not vary simply with ϵ. In particular, the shape and extent of the gyroid region differ greatly between the three chemistries; in the S/EP system, this region disappears into a cusp at moderate segregation strengths ($\chi N \approx 24$). Our findings indicate that factors other than ϕ, χN, and ϵ do influence the free energy of diblock copolymer mesophases and their regions of stability.

Introduction

Block copolymer morphologies have been studied intensively for the past three decades.[1,2] By examining a series of diblocks of the same chemistry but varying composition (block ratio), a "phase diagram" can be constructed, where the volume fraction of one block (ϕ) serves as the abscissa and the segregation strength between the blocks (χN, where χ is the Flory−Huggins interaction parameter and N the total degree of polymerization) as the ordinate. So extensive is the body of work on styrene−butadiene and styrene−isoprene diblocks that the phase diagrams for these styrene−diene systems are often considered to be representative of those for any flexible-chain block copolymer. However, Vavasour and Whitmore[3] showed via self-consistent-field (SCF) calculations that the positions of the phase boundaries (e.g., the curve dividing a mesophase showing a body-centered-cubic packing of spheres from that showing a hexagonal packing of cylinders) depends on the conformational asymmetry of the polymer, which is essentially a measure of the unperturbed sizes of the two blocks relative to their volume fractions.[4] Conformational asymmetry is typically characterized through a parameter ϵ:

$$\epsilon \equiv \frac{\rho_B}{\rho_A}\left(\frac{R_{g,B}{}^2/M_B}{R_{g,A}{}^2/M_A}\right) \tag{1}$$

Here, $R_{g,i}{}^2/M_i$ (where R is the mean-square radius of gyration and M the molecular weight) is a measure of the chain stiffness of homopolymer i; ρ_i is the mass density of homopolymer i, and subscripts A and B denote the two blocks. This SCF treatment for conformationally asymmetric polymers was subsequently refined and extended to cover all the known equilibrium phases exhibited by diblocks.[5] For the ranges of ϵ typically found in flexible-chain block copolymers, conformational asymmetry is predicted to skew all the boundary lines dividing ordered phases to one side of the phase diagram, while having little effect on the order−disorder transition (ODT) boundary. Also, the mesophases in the center of the diagram (gyroid and lamellae) are predicted[5] to occur over about the same width (range of volume fractions of one block) as ϵ is changed, though the values bounding each range will change with ϵ.

The concept of conformational asymmetry was an important advance in highlighting differences between the phase diagrams of different block copolymers and in explaining their origin. The most obvious effect of conformational asymmetry—the skewing, or lack of mirror symmetry about $\phi = {}^1/_2$ in real phase diagrams—has been confirmed for block copolymers of several chemistries[6−8] and was, in fact, anticipated by the strong-segregation theory of Helfand and Wasserman.[9] But the larger question of whether these three parameters—ϕ, χN, and ϵ—are sufficient to uniquely describe diblock copolymer phase behavior in the long-chain limit remains experimentally untested. In the present work, we address this question by comparing in detail the phase diagrams of polymers with different ϵ but similar molecular weights (so that the influence of fluctuations[6] should be similar in all cases). The large body of work on styrene−isoprene (S/I) diblocks[10] provides a solid base for comparison, while the simplest related materials are hydrogenated derivatives of such styrene−isoprene diblocks. By using appropriate catalysts,[11] it

* To whom correspondence should be addressed.
† Present address: Bristol-Myers Squibb Pharmaceutical Research Institute, P.O. Box 191, New Brunswick, NJ 08903.
‡ Present address: Dow-DuPont Elastomers L.L.C., P.O. Box 400, Plaquemine, LA 70765.

10.1021/ma991156q CCC: $19.00
Published on Web 04/12/2000

Table 1. Characteristics of S/I Diblocks

	materials	w_I	3,4 I (%)[b]	ϕ_I[c]	M_w (kg/mol)	T_{ODT} (°C)	morphology[d]
series A	S/I 10/15[a]	0.607	6.6	0.643	24.4	149 ± 1	gyroid
	S/I 10/16	0.622	6.9	0.658	25.6	171 ± 1	gyroid
	S/I 8/17	0.665	6.5	0.699	25.2	158 ± 1	cylinders
series B	S/I 8/11	0.592	7.2	0.629	19.4	97 ± 1	lamellae
	S/I 9/14	0.613	7.1	0.649	22.1	121 ± 1	lamellae[e]
	S/I 7/13	0.659	6.7	0.693	20.3	103 ± 1	cylinders

[a] Molecular weight of each block in kg/mol. [b] Content of 3,4-type addition in the isoprene block. [c] Bulk densities[23] of PS (0.969 g/cm^3) and PI (0.830 g/cm^3) homopolymers at 140 °C used to calculate volume fractions; the small temperature dependence of ϕ is neglected throughout this work. [d] Equilibrium morphology for series A at 140 °C and for series B at 95 °C. [e] Shows L→ G order−order transition (OOT) at 101 °C; other samples show no OOT.

is possible to saturate the isoprene (I) blocks to ethylene-*alt*-propylene (EP), while leaving the styrene (S) blocks untouched, or to saturate both I to EP and S to vinylcyclohexane (VCH). This provides three sets of materials (S/I, S/EP, VCH/EP) from one set of parent polymers, where all three are intrinsically matched in chain length but differ substantially in ϵ. Moreover, the improved thermooxidative stability of EP over I allows S/EP and VCH/EP diblocks to be studied over a wide temperature range without degradation. We concentrate on the portion of the phase diagram that contains bounding lines between the cylindrical (C), gyroid (G), and lamellar (L) phases. In this composition range, these three morphologies are predicted to have rather similar free energies,[12] meaning that any nonuniversality (differences in the equilibrium mesophase not simply attributable to ϕ, χN, and ϵ) would be most clearly manifested in this region.

Experimental Section

Two sets of S/I diblocks were synthesized for this work, via sequential anionic polymerization in hydrocarbon solvents; each set has a nearly constant total molecular weight but a varying composition (S/I ratio), as given in Table 1. Materials are identified by their block chemistries and the approximate molecular weights of the two blocks, in kg/mol. The polymers in series A ($M \approx 25$ kg/mol) were synthesized at Dexco Polymers, isoprene block first; those in series B ($M \approx 20$ kg/mol) were synthesized using high-vacuum techniques at Princeton, styrene block first. Table 1 also lists the microstructure of the isoprene block for each diblock, obtained from ^{1}H nuclear magnetic resonance (NMR); the I block contains approximately 7% 3,4 addition in all cases. Obtaining a highly reproducible measure of block copolymer composition (weight fraction isoprene, w_I) was critical for this work; using ^{1}H NMR in *d*-$CHCl_3$ and making repeated measurements on different aliquots of the same polymers, we determined the precision of the composition measurements to be ±0.2 wt % S. The initiator (butyl) end group was neglected in calculating the compositions. Molecular weights of the diblocks were obtained by gel permeation chromatography (GPC) in toluene, by correcting the apparent molecular weight for the variation in hydrodynamic volume with polymer composition.[13] Two of the polymers as synthesized contained detectable terminated first block and so were fractionated using toluene/methanol to extract a pure diblock product (no detectable homopolymer, <0.2 wt %) prior to detailed analysis. All polymers showed narrow monomodal molecular weight distributions, with apparent polydispersities of less than 1.04 (close to the GPC column limit).

The hydrogenation procedures have been reported in detail previously.[11] In brief, the isoprene-selective hydrogenation employs a catalyst prepared by reducing nickel octanoate with triethylaluminum,[14] while the nonselective hydrogenation employs palladium metal[15] supported on either $CaCO_3$ or $BaSO_4$. (The type of support had no noticeable effect on the extent or rate of hydrogenation.) When necessary, hydrogenations were repeated until no detectable unsaturation remained by ^{1}H NMR (<0.2 wt % in I block, <0.4 wt % in S block). GPC traces of the products superposed on those of the precursors (with a shift in elution time due to the change in hydrodynamic volume), indicating no detectable chain scission during hydrogenation.

One-dimensional SAXS data were collected with a compact Kratky camera and a position-sensitive detector (Braun OED-50M). The data were reduced using previously reported procedures[16] to desmeared absolute intensity versus the scattering vector $q = 4\pi \sin \theta/\lambda$, where λ is the Cu Kα radiation wavelength and 2θ is the scattering angle. Static SAXS data were acquired at different temperatures through the use of a microprocessor-controlled hot stage.[17]

In constructing a phase diagram, it is essential to ensure insofar as possible that the morphology determined at any point (ϕ and T or χN) is the equilibrium one. The S/I and VCH/EP diblocks studied here all have thermally accessible ODTs, so these materials were first heated to at least 20 °C above the order−disorder transition temperature (T_{ODT}) and then quenched to the target temperature. The S/EP diblocks, however, remain ordered up to the 300 °C limit of the hot stage. CCl_4 is a nearly neutral solvent for styrene−olefin block copolymers,[18] so 5 wt % solutions of polymer in CCl_4 were prepared, and the solvent was evaporated gradually over ca. 2 days, followed by drying at 160 °C under vacuum. The thermoreversible order−order transitions observed for these S/EPs (see Results and Discussion) indicate that the polymers have sufficient mobility at the temperatures of interest to reach their equilibrium morphologies. Binary blends (whether of S/I, VCH/EP, or S/EP diblocks) were prepared by codissolution at 5 wt % in CCl_4, cast into films as for the S/EP diblocks, and subsequently thermally treated as for the analogous pure diblocks. The single sharp primary peak observed in the SAXS profiles for all blends suggests the absence of macroscopic phase separation, in accord with theoretical expectations[19] for diblocks so closely matched in composition and molecular weight.

Results and Discussion

Table 1 lists the equilibrium morphologies of all six S/I diblocks[20] as well as the ODT temperatures determined on heating as described previously.[11,17] The morphology is easily identified through the ratios of the q values of the first two peaks (though the intensity of peaks beyond the primary at q^* is often weak due to the proximity of the order−disorder transition): q^*:q_2 = 1:2 for lamellae, 1:$\sqrt{4/3}$ for gyroid, and 1:$\sqrt{3}$ for cylinders. Only representative SAXS patterns will be shown here as examples of how phase diagrams were constructed, but many additional patterns can be found elsewhere.[21] Upon dual hydrogenation (conversion from S/I to VCH/EP), both 10/16 and 10/15 change from gyroid to lamellae, as indicated in Table 2. This is somewhat counterintuitive, as the VCH/EP diblocks are actually more asymmetric than their S/I precursors; this observation hints at the influence of conformational asymmetry.[22] To locate the VCH/EP phase boundaries more precisely, we made binary blends of the 8/17

Table 2. Characteristics of S/EP and VCH/EP Diblocks

	materials	ϕ_{EP}[a]	T_{ODT} (°C)	morphology[b]	q^* (nm^{-1})[c]
series A	VCH/EP 10/15	0.639	164 ± 2	lamellae	0.284
	VCH/EP 10/16	0.654	178 ± 2	lamellae	0.277
	VCH/EP 8/17	0.695	170 ± 2	cylinders	0.300
series B	S/EP 8/11	0.642	>300	lamellae/gyroid	0.260
	S/EP 9/14	0.667	>300	lamellae/gyroid	0.238
	S/EP 7/13	0.709	>300	lamellae/cylinders	0.272

[a] Bulk densities[23] of PS (0.969 g/cm^3), PVCH (0.920 g/cm^3), and PEP (0.790 g/cm^3) homopolymers at 140 °C used to calculate volume fractions; the small temperature dependence of ϕ is neglected throughout this work. [b] Equilibrium morphology over temperature range examined; more than one entry indicates an OOT within the experimental temperature range. [c] Primary SAXS peak position at 140 °C.

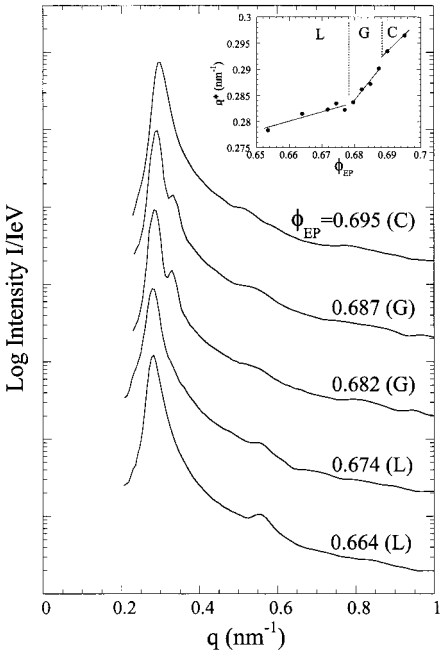

Figure 1. SAXS profiles (log intensity scale) at 140 °C for representative members in a series of binary blends of VCH/EP 8/17 and VCH/EP 10/16; volume fraction of EP (ϕ_{EP}) indicated on curves, along with morphology (L = lamellae, G = gyroid, C = cylinders). Profiles are shifted along the intensity axis for clarity. Inset: primary peak position at 140 °C for all blends in this series. Note small but measurable changes in q^* or $dq^*/d\phi_{EP}$ at the phase boundaries.

(cylinders) and 10/16 (lamellae) diblocks at various compositions. SAXS profiles of representative blends in this series at 140 °C are shown in Figure 1, where the inset tracks the primary peak position q^* as a function of ϕ_{EP}. By inspection of the SAXS profiles and from the changes in q^*, the L/G boundary is located at ϕ_{EP} = 0.679 and the G/C boundary at ϕ_{EP} = 0.689, each with a precision of ±0.001. Similar measurements on blends of S/I 8/17 and 10/16 located the G/C phase boundary at ϕ_I = 0.669. Though we did not have a lamellar S/I of appropriate molecular weight to use in blending, previous work by Khandpur et al.[10] has shown the gyroid window to have a compositional width of 0.03 in S/I diblocks, so we would expect the L/G phase boundary in S/I to occur near ϕ_I = 0.64.

If ϕ, χN, and ϵ are a sufficient set of variables to describe block copolymer phase behavior, then it should be possible to combine all block copolymer phase diagrams (in the long-chain limit) into a single three-dimensional phase diagram, where the axes are ϕ, χN, and ϵ. The usual 2D phase diagram (χN vs ϕ for a particular diblock system, with constant ϵ) would thus be a cut of this 3D phase diagram taken perpendicular to the ϵ axis. It is equally instructive to take a cut perpendicular to the χN axis, yielding a 2D phase diagram where the axes are ϵ and ϕ; however, such a comparison requires the polymers of different chemistry (ϵ) to be matched in χN, a difficult condition to meet experimentally. When comparing segmental interactions in systems having different chemistries, it is most convenient to use the interaction energy densities, X. We have previously[11] estimated X for the S/I, VCH/EP, and S/EP systems; following this approach, and using data reported in the literature[11,24] as well as some values measured for this work,[21] we obtained[21] the following expressions for X (J/cm^3):

$$X_{S/I} = -0.30 + 1013/T\ (K) \quad (2)$$

$$X_{VCH/EP} = 0.46 + 616/T\ (K) \quad (3)$$

$$X_{S/EP} = 0.57 + 1655/T\ (K) \quad (4)$$

From these expressions, χN can be evaluated for any such diblock, without introducing an arbitrary reference volume, from

$$\chi N = X(M/\rho RT) \quad (5)$$

where R is the gas constant and ρ, the bulk density of the diblock, can be obtained from the known melt densities[23] and thermal expansion coefficients[24] of the constituent blocks. Equations 2−4 are consistent with previous reports that χN for an S/I and an equivalent VCH/EP are similar[24] in the temperature range studied here, while χN for an equivalent S/EP is much larger.[11] To achieve a value of χN in the S/EP system comparable to that for the series A S/I and VCH/EP diblocks, we use polymers of 20% lower molecular weight (series B vs series A) and a higher temperature (300 vs 140 °C). From eqs 2−5, the χN products for series A S/I and VCH/EP diblocks at 140 °C lie in the range 16.8−18.3, while χN values for the series B S/EP diblocks at 300 °C range from 17.6 to 20.0, close enough for a meaningful comparison.

Literature values[23] of ρ_i and $R_{g,i}^2/M_i$ yield the following values of ϵ at 140 °C: $\epsilon_{S/I}$ = 0.81, $\epsilon_{S/EP}$ = 0.64, and $\epsilon_{VCH/EP}$ = 0.45. (Though ϵ is actually a temperature-dependent quantity, the variation is modest over the temperature ranges explored here.) Here, the I or EP block is defined as block A in eq 1, so as to yield ϵ < 1 in accordance with convention.[3] The $\chi N-\phi$ phase diagrams will be plotted against ϕ_A. Figure 2 shows what would be essentially a cut of the hypothetical 3D phase diagram at a fixed χN value (≈18); the axes are ϵ and ϕ_A, and data for S/I, S/EP, and VCH/EP diblocks are shown. Superimposed on the experimental data are the results of SCF calculations[5] at this value of χN and three discrete values of ϵ, connected with smooth dashed curves. The SCF calculations reproduce the broadest

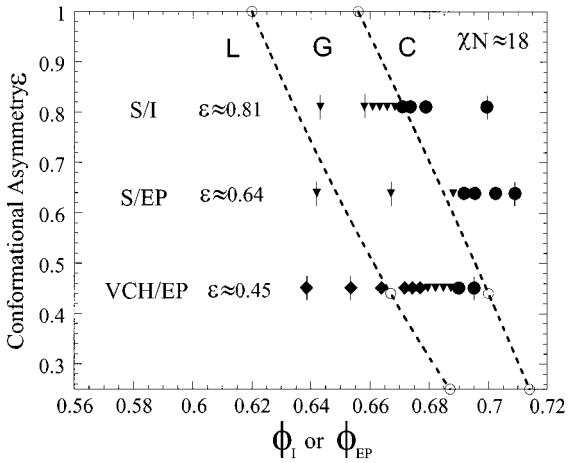

Figure 2. Phase diagram at constant χN (18.4 ± 1.6) for diblocks of varying conformational asymmetry: S/I ($\epsilon = 0.81$), S/EP ($\epsilon = 0.64$), and VCH/EP ($\epsilon = 0.45$). Experimental points are shown with filled symbols: lamellae (◆, L), gyroid (▼, G), and cylinders (●, C). Points with a vertical strike through them are pure diblocks; other points are blends of the two pure diblocks which they lie between. The three pairs of open circles represent the results of SCF calculations[5] for the L/G and G/C phase boundaries at $\chi N = 18$ and discrete values of $\epsilon = 0.25$, 0.44, and 1.0; these points are connected with dashed lines as guides to the eye.

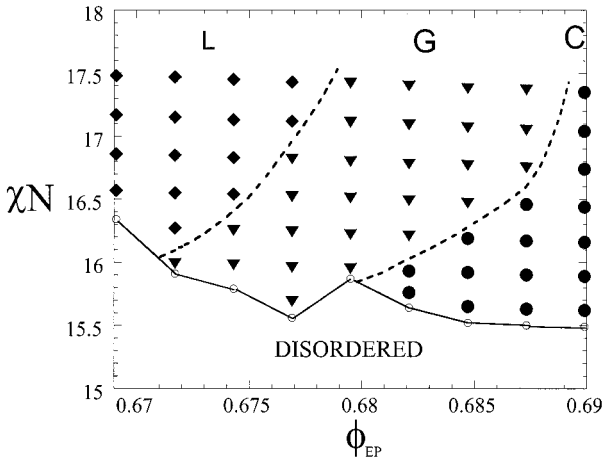

Figure 3. Phase diagram for VCH/EP ($\epsilon = 0.45$), varying χN and ϕ_{EP}. VCH/EP 8/17 and 10/16 (which have ϕ_{EP} lying outside the range of this diagram, see Table 2) were blended together to cover this composition range. Morphologies are shown with filled symbols: lamellae (◆, L), gyroid (▼, G), and cylinders (●, C). Open circles connected with solid lines represent the location of the order−disorder transitions; dashed curves are drawn in the approximate positions of the phase boundaries between different ordered mesophases.

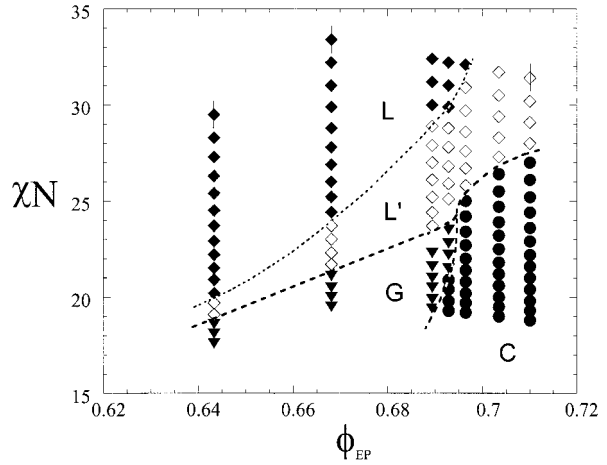

Figure 4. Phase diagram for S/EP ($\epsilon = 0.64$), varying χN and ϕ_{EP}. Morphologies are shown with filled symbols: lamellae (◆, L), gyroid (▼, G), and cylinders (●, C). Specimens denoted L′ (◇) show a significant attenuation of the second-order SAXS peak, as discussed in the text. Materials whose symbols at the highest χN value contains a vertical overstrike are pure diblocks; other materials are blends of the two pure diblocks which they lie between. Dashed curves are drawn in the approximate positions of phase boundaries between different ordered mesophases.

trend in the data: the skewing of the phase boundaries to higher ϕ_A (where A is the conformationally larger block) with increasing ϵ. The agreement between theory and experiment is not entirely quantitative, however, and this is most evident by comparing the compositional "width" of the gyroid window. The SCF calculations predict a gyroid window that extends over roughly 0.03 in ϕ for any ϵ; while this is observed[10] for S/I, the gyroid window for S/EP extends over at least 0.045 in ϕ at this χN, while that for VCH/EP extends over a mere 0.010 in ϕ.

Examination of the full phase diagrams for S/I, VCH/EP, and S/EP reveals more substantial differences. The experimental phase diagram for VCH/EP is shown in Figure 3. The high resolution provided by the fine temperature and composition increments used in constructing this diagram reveals the existence of numerous L/G and G/C order−order transitions (OOTs). All of these order−order transitions were confirmed to be thermoreversible; cooling the specimens to 10 °C or more below the OOT temperature caused the transformation to completely reverse within a day. In the VCH/EP system, the slopes of the order−order phase boundaries near the order−disorder transition are rather shallow, approximately 200 for the L/G boundary and 120 for the G/C boundary at $\chi N - (\chi N)_{ODT} \approx 1$. From the OOT temperatures reported by Khandpur et al.,[10] using eqs 2 and 5 to calculate χN, slopes for the L/G and G/C boundaries at $\chi N - (\chi N)_{ODT} \approx 4$ in S/I are calculated as 600 and 400. Note that the magnitudes of these slopes are directly affected by the values of the $1/T$ coefficients in eqs 2 and 3, quantities which certainly have some experimental uncertainty, as is evident when values extracted from different methods are compared.[25] However, the relative uncertainty in the $1/T$ coefficients cannot be as large as the factor of 3 required to bring the S/I and VCH/EP boundary slope values into agreement, as side-by-side measurements of matched S/I and VCH/EP diblocks[24] clearly show the weaker temperature dependence of X in VCH/EP.

The experimental phase diagram for S/EP looks quite different from those for S/I and VCH/EP, as shown in Figure 4. One notable feature is the shape of the gyroid phase envelope, which comes to a very sharp cusp at $\chi N \approx 24$ and $\phi_{EP} = 0.694$. A second distinctive feature is found in the lamellar region, which we have divided into two parts labeled "L" and "L′". Samples in the L region show the SAXS patterns expected for a lamellar structure. Specimens in the L′ region also show SAXS patterns which one would normally identify as lamellar, but with a second-order peak having an intensity much reduced from that exhibited by specimens in the L region. Also, oriented specimens of the L′ structure show off-equatorial maxima in their 2D SAXS patterns.[21] These features are reminiscent of the "perforated lamellar" and "modulated lamellar" morphologies,[26] which

have been shown to be metastable structures[27,28] occurring in regions where the gyroid phase is stable. However, in our case, all the types of transitions shown in Figure 4 (L ↔ L′, L′ ↔ G, L′ ↔ C) were confirmed to be thermoreversible; that G transforms readily to L′ indicates that G is *not* the equilibrium structure where we find L′. The exact nature of the L′ structure is currently under investigation by electron microscopy[29] but is beyond the scope of the present paper, where we are concerned principally with the shape of the gyroid region.

For S/EP, the slope of the G/C phase boundary at $\chi N = 20$ is rather steep (≈600), while the slope of the L′/G boundary is much shallower (≈100), comparable to the boundary slopes in the VCH/EP system. These grossly different slopes combine to produce the cusp at $\chi N \approx 24$ and $\phi_{EP} = 0.694$ and yield a gyroid window whose width changes drastically over a relatively narrow range of χN (18−24). This contrasts with the gyroid windows in S/I and VCH/EP, whose widths vary little over a few units in χN. When considering the S/EP system, a useful point for comparison is the work of Hajduk et al.[30] on a styrene−(ethylene-*co*-butene) diblock, S/EB, at $\chi N \approx 30$. S/EB is chemically similar to S/EP and has a similar value of ϵ ($\epsilon_{S/EB} = 0.68$ at 140 °C for this EB microstructure[23]). This S/EB diblock showed a direct thermoreversible L ↔ C transition (though with some temperature hysteresis); no G phase was observed, though such a bicontinuous cubic was searched for, as it is expected to lie between the L and C phases according to SCF calculations[31,32] at these segregation strengths. If a G region exists for S/EB diblocks, then it must also "pinch off" at relatively low χN, as we find for the G region in S/EP.

Conclusions

Significant differences in the widths and shapes of the gyroid region were found between S/I, S/EP, and VCH/EP diblocks. In particular, the compositional width of the gyroid region near the ODT is approximately 3% in S/I ($\epsilon = 0.81$), 5% in S/EP ($\epsilon = 0.64$), and only 1% in VCH/EP ($\epsilon = 0.45$). Also, while the L/G and G/C phase boundaries in plots of χN vs ϕ are roughly parallel in the S/I and VCH/EP systems, leading to gyroid regions whose widths change little with segregation strength, the S/EP system shows a broad G window near the ODT which closes off completely at moderate segregations ($\chi N \approx 24$). Thus, the phase diagrams for S/I, VCH/EP, and S/EP cannot be joined together to make a sensible three-dimensional (ϕ, χN, and ϵ) phase diagram. These results conflict with recent SCF calculations,[5] which suggest that the G window should have approximately a 3% compositional width in any flexible-chain system, depending only very weakly on ϵ.

These deviations lead us to conclude that ϕ, χN, and ϵ are not sufficient to completely and quantitatively describe block copolymer phase diagrams at a constant molecular weight. Other factors evidently contribute to the free energy of block copolymer mesophases and influence the composition range over which they are stable (here, most notably for the gyroid region). Though we have not yet identified what these factors are, one possibility is that the differences in phase behavior are related to differences in how real polymers (S, VCH, I, EP) depart from the Gaussian chain statistics which the SCF treatment assumes. A second possibility is suggested by the absence of a gyroid phase in both S/EP and S/EB diblocks at moderate segregation strengths. The S/EP and S/EB systems have a similar[11] χ, hence similar local as well as global energetics, suggesting that the details of the A−B interactions at the interface may play a role.

Acknowledgment. This work was supported by the Princeton Center for Complex Materials, a National Science Foundation Materials Research Science and Engineering Center (DMR-9400362 and DMR-9809483), and by the Polymers Program of the National Science Foundation (DMR-9711436).

References and Notes

(1) Bates, F. S.; Fredrickson, G. H. *Phys. Today* **1999**, *52*, 32.
(2) Hamley, I. W. *The Physics of Block Copolymers;* Oxford University Press: New York, 1998.
(3) Vavasour, J. D.; Whitmore, M. D. *Macromolecules* **1993**, *26*, 7070.
(4) Almdal, K.; Koppi, K. A.; Bates, F. S.; Mortensen, K. *Macromolecules* **1992**, *25*, 1743.
(5) Matsen, M. W.; Bates, F. S. *J. Polym. Sci., Part B: Polym. Phys.* **1996**, *35*, 945.
(6) Bates, F. S.; Schulz, M. F.; Khandpur, A. K.; Förster, S.; Rosedale, J. H.; Almdal, K.; Mortensen, K. *Faraday Discuss.* **1994**, *98*, 7.
(7) Winey, K. I.; Gobran, D. A.; Xu, Z.; Fetters, L. J.; Thomas, E. L. *Macromolecules* **1994**, *27*, 2392.
(8) Mai, S.-M.; Fairclough, J. P. A.; Hamley, I. W.; Matsen, M. W.; Denny, R. C.; Liao, B.-X.; Booth, C.; Ryan, A. J. *Macromolecules* **1996**, *29*, 6212.
(9) Helfand, E.; Wasserman, Z. R. In *Developments in Block Copolymers-1*; Goodman, I., Ed.; Applied Science Publishers: New York, 1982; p 99.
(10) Khandpur, A. K.; Förster, S.; Bates, F. S.; Hamley, I. W.; Ryan, A. J.; Bras, W.; Almdal, K.; Mortensen, K. *Macromolecules* **1995**, *28*, 8796.
(11) Adams, J. L.; Quiram, D. J.; Graessley, W. W.; Register, R. A. *Macromolecules* **1997**, *31*, 2201.
(12) Matsen, M. W.; Bates, F. S. *Macromolecules* **1996**, *29*, 7641.
(13) Sebastian, J. M.; Register, R. A., to be submitted to *J. Appl. Polym. Sci.*
(14) Hahn, S. F. *J. Polym. Sci., Part A: Polym. Chem.* **1992**, *30*, 397.
(15) Gehlsen, M. D.; Bates, F. S. *Macromolecules* **1993**, *26*, 4122.
(16) Register, R. A.; Bell, T. R. *J. Polym. Sci., Part B: Polym. Phys.* **1992**, *30*, 569.
(17) Adams, J. L.; Quiram, D. J.; Graessley, W. W.; Register, R. A.; Marchand, G. R. *Macromolecules* **1996**, *29*, 2929.
(18) Hsieh, W. V. B.S.E. Thesis, Princeton University, 1993.
(19) Matsen, M. W.; Bates, F. S. *Macromolecules* **1995**, *28*, 7298.
(20) Note that there appears to be a slight inconsistency between the two series of S/I diblocks. S/I 9/14, compared with S/I 10/15, is slightly more asymmetric and less strongly segregated, yet it is lamellar at 100 °C and below, where S/I 10/15 is gyroid. A similar difference was reflected in the phase boundaries of the S/EP derivatives of these polymers,[21] where series A polymers behave as if they had slightly less styrene (or series B polymers slightly more) than their compositions would indicate. We believe that this difference is a consequence of the method of synthesis, in particular the location of the butyl residue from the initiator, which is at the end of the I block in series A and the S block in series B. The mass of this end group, though small, translates to half the difference in composition between S/I 9/14 and S/I 10/15. The measurable effect of this seemingly minuscule difference highlights how delicately balanced the free energies are in this composition region.
(21) Lai, C. Ph.D. Thesis, Princeton University, 1999.
(22) Sakurai, S.; Hashimoto, T.; Fetters, L. J. *Macromolecules* **1995**, *28*, 7947.
(23) Fetters, L. J.; Lohse, D. J.; Richter, D.; Witten, T. A.; Zirkel, A. *Macromolecules* **1994**, *27*, 4639.
(24) Balsara, N. P.; Lin, C. C.; Dai, H. J.; Krishnamoorti, R. *Macromolecules* **1994**, *27*, 1216.
(25) Adams, J. L.; Graessley, W. W.; Register, R. A. *Macromolecules* **1994**, *27*, 6026.

(26) Hamley, I. W.; Koppi, K. A.; Rosedale, J. H.; Bates, F. S.; Almdal, K.; Mortensen, K. *Macromolecules* **1993**, *26*, 5959.
(27) Hajduk, D. A.; Takenouchi, H.; Hillmyer, M. A.; Bates, F. S.; Vigild, M. E.; Almdal, K. *Macromolecules* **1997**, *30*, 3788.
(28) Vigild, M. E.; Almdal, K.; Mortensen, K.; Hamley, I. W.; Fairclough, J. P. A.; Ryan, A. J. *Macromolecules* **1998**, *31*, 5702.
(29) Loo, Y.-L.; Register, R. A., work in progress.
(30) Hajduk, D. A.; Gruner, S. M.; Rangarajan, P.; Register, R. A.; Fetters, L. J.; Honeker, C.; Albalak, R. J.; Thomas, E. L. *Macromolecules* **1994**, *27*, 490.
(31) Matsen, M. W.; Bates, F. S. *Macromolecules* **1996**, *29*, 1091.
(32) Matsen, M. W.; Bates, F. S. *J. Chem. Phys.* **1997**, *106*, 2436.

MA991156Q